



Cite this: DOI: 10.1039/c8lc00098k

Biodegradable 3D printed polymer microneedles for transdermal drug delivery†

Michael A. Luzuriaga,^a Danielle R. Berry,^a John C. Reagan,^b Ronald A. Smaldone^{*a} and Jeremiah J. Gassensmith^{ib*ab}

Biodegradable polymer microneedle (MN) arrays are an emerging class of transdermal drug delivery devices that promise a painless and sanitary alternative to syringes; however, prototyping bespoke needle architectures is expensive and requires production of new master templates. Here, we present a new micro-fabrication technique for MNs using fused deposition modeling (FDM) 3D printing using polylactic acid, an FDA approved, renewable, biodegradable, thermoplastic material. We show how this natural degradability can be exploited to overcome a key challenge of FDM 3D printing, in particular the low resolution of these printers. We improved the feature size of the printed parts significantly by developing a post fabrication chemical etching protocol, which allowed us to access tip sizes as small as 1 μm. With 3D modeling software, various MN shapes were designed and printed rapidly with custom needle density, length, and shape. Scanning electron microscopy confirmed that our method resulted in needle tip sizes in the range of 1–55 μm, which could successfully penetrate and break off into porcine skin. We have also shown that these MNs have comparable mechanical strengths to currently fabricated MNs and we further demonstrated how the swellability of PLA can be exploited to load small molecule drugs and how its degradability in skin can release those small molecules over time.

Received 27th January 2018,
Accepted 5th March 2018

DOI: 10.1039/c8lc00098k

rsc.li/loc

Introduction

Hypodermic needles have been used clinically for more than 150 years and are the most common drug delivery devices. Although effective, hypodermic needles cause pain, elicit phobias in patients, require training and generate biohazardous waste.^{1,2} Polymer microneedle (MN) arrays are flexible patterned grids of sharp micron-sized protrusions capable of delivering therapeutic agents into the skin and are notably pain-free. MNs have gained attention in recent years as a minimally invasive and cost effective method to enhance drug delivery.^{3–5} In an array, polymer MNs can act as a passive drug delivery system with the potential to improve drug efficacy owing to several intrinsic advantages: namely they (i) can elicit a higher immunogenic response,^{6–10} (ii) inhibit microbial entrance at the injection site,¹¹ (iii) can be administered at home by unskilled caregivers,^{12,13} (iv) have the capacity to improve the shelf life of drugs,^{14–16} (v) have the capability for high loading capacity,^{17,18} and (vi) have flexibility in material

composition that permits smart drug delivery systems.^{19–22} This flexibility means polymer MN arrays can be tailored to the therapeutic used and the intended application using different MN architectures. At their most basic, microneedles are used to perforate skin to permit faster passive diffusion of a topically applied drug directly into the dermis. More complex architectures have been discussed in several excellent articles and reviews^{23–32} though the most common architectures in literature either involve coating drug onto the surface of the MNs to allow instant dosing upon tissue penetration or trapping both small- and large-molecular weight agents^{33,34} within the polymeric matrix of the MNs. In these latter formulations, the MNs can be broken off into the skin and the gradual dissolution of the needle within the skin concomitantly releases drug.

Fabrication of these polymeric MNs is typically accomplished with a micromolding process that enables the use of the mold several times.³⁵ This process typically involves creation of a single master template, which is then used to cast all the subsequent MNs.³⁶ Although template driven fabrication has precise control over shape and size, the startup costs associated with it are high. Template fabrication is generally complicated, needs a controlled environment of low particles, and requires expensive photolithography and etching equipment.³⁷ Template fabrication becomes problematic when any modification becomes necessary to the MN. This is

^a Department of Chemistry and Biochemistry, University of Texas at Dallas, 800 West Campbell Road, Richardson, TX 75080-3021, USA.

E-mail: ronald.smaldone@utdallas.edu, gassensmith@utdallas.edu

^b Department of Bioengineering, University of Texas at Dallas, 800 West Campbell Road, Richardson, TX 75080-3021, USA

† Electronic supplementary information (ESI) available. See DOI: 10.1039/c8lc00098k

acceptable for designs that are ready for mass production, but is expensive for screening new designs. Alternative methods to photolithography have been reported to add flexibility and productivity such as two photon polymerization³⁸ and bulk micromachining.³⁹ However, these methods are still considered to be time consuming and expensive in the production of prototype MNs.

Additive manufacturing, more commonly known as 3D printing, is a method of fabricating physical parts from a digital model generated using computer aided design software by adding materials layer by layer.⁴⁰ The 3D printer's ability to allow users to produce objects on demand has proven useful in construction,⁴¹ automotive⁴² and aerospace manufacturing,⁴³ and biomedical applications.^{44,45} Scientists are beginning to implement 3D printing in the research laboratory as a tool for rapid prototyping,^{46–48} device fabrication,⁴⁹ self-healing polymers for improved mechanical strength,^{50–52} and developing scaffolds for tissue engineering.^{53,54} 3D printers commonly used for printing plastic materials include fused deposition modeling (FDM),^{51,55–57} selective laser sintering (SLS),^{58,59} and stereolithography (SLA).^{58,60} SLS and SLA printers are capable of producing features smaller than 100 μm , however, these printers can be costly⁶¹ and most materials are not biocompatible. For instance, the photo-initiators required in the SLA printing process are toxic and are incompatible for transdermal drug delivery.^{62–64}

FDM is versatile, cost effective, and can print renewable and biodegradable materials, such as polylactic acid (PLA) and polyvinyl alcohol, which are approved by the Food and Drug Administration (FDA) for use in dissolvable stitches.⁶⁵ However, a major limitation is that the resolution of FDM is

lower than other printing methods and generally incapable of making fine structures like MNs. Studies comparing hypodermic needles and MNs have been conducted and the optimal length, width, thickness, and the number of MNs in an array that cause pain in humans have been determined.^{66,67} These studies concluded that MNs with lengths up to 1450 μm , widths of 465 μm , thicknesses of 100 μm , and tip sizes of less than 75 μm cause less pain than a 26-gauge hypodermic needle and that the main factor in pain was the amount of MNs in an array. Even under ideal conditions, extrusion from the print head of a commercially available FDM printer is unlikely to produce features this fine. Herein, we show a new method that combines FDM with a post-fabrication etching step to yield ideally sized and shaped needles that are able to insert, break off, and deliver small molecules into skin without the need of a master template or mold (Fig. 1).

Results and discussion

At a minimum, the 3D printed MN array should be expected to effectively penetrate skin, which would be sufficient to permit drug delivery by coating a therapeutic onto the surface of the needles. However, we sought to go further to maximize potential use and focused on a design that would satisfy an additional three objectives: (i) produce a break-away architecture such that the individual needles in the array break off with an applied transverse force leaving them embedded in the skin; (ii) it should be possible to “load” the needle with a small molecule drug-like indicator after printing; (iii) this drug should diffuse from the embedded broken needle over time within the skin. We thus narrowed our choice of thermoplastic polymer to PLA, a common filament choice for

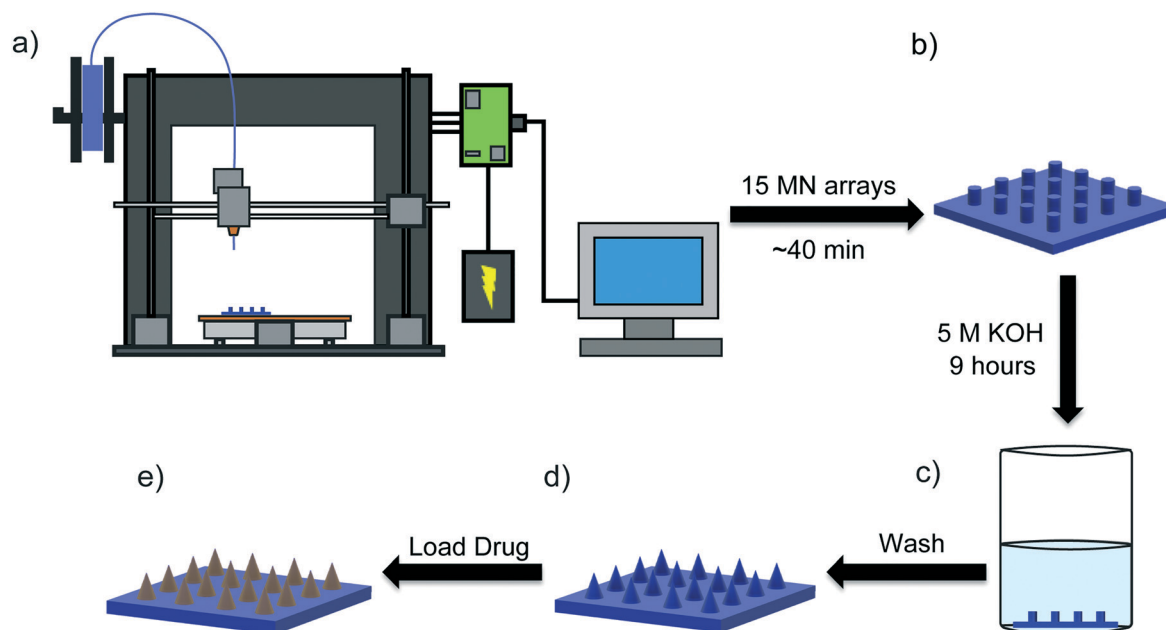


Fig. 1 Schematic illustration of a) FDM 3D printer used for microneedle production b) 3D printed microneedles as fabricated c) chemically etched microneedles using an alkaline solution d) etched microneedles after washing with water e) microneedles after drug loading.

FDM printing. With the filament choice in hand, over the course of our investigation, we tested seven MN shapes, which are schematically illustrated in Table 1, to print an array which meets the above criteria. Type 1 and type 2 were tested to obtain sharp tips, but we found the sharp features exceeded the resolution of even small diameter hot end (350 μm) and these designs were poorly replicated by the 3D printer. Even more gradual changes, illustrated as type 3 and 4, were malformed after printing, owing to the filament deposition process. Overall, types 1–4 showed that gradual changes could not be achieved because of poor adhesion between extruded layers, a common problem that occurs in FDM printing of small structures. Owing to this limitation, we modified our approach in needle types 5–7 by using terraced layers rather than gradual sloping, which proved to be successful. With a 350 μm hot end, MNs ranging in lengths from 200–2500 μm , widths from 400–600 μm , thicknesses from 400–600 μm , and tip diameters from 170–220 μm could be produced (Fig. 2a–c and S1†). These measurements exceed the optimal dimensions for ideal MNs, an expected result given the known resolution limitations of FDM printing.

PLA is a biocompatible polyester produced from renewable lactic acid and can be degraded into smaller fragments through hydrolysis. The rate of degradation is proportional to the strength of the acidity or alkalinity of the surrounding media. Skin, for instance, is mildly acidic,⁶⁸ which makes PLA an attractive material for use in dissolvable stitches. We thus wondered if we could etch our low resolution MNs to dimensions that would be appropriate for painless skin penetration. Aqueous potassium hydroxide (KOH) solutions were made at 1, 3, 5, 7, and 9 M concentrations and the etching rate of the as fabricated MNs were evaluated *via* optical and scanning electron microscopy (SEM) to determine the change

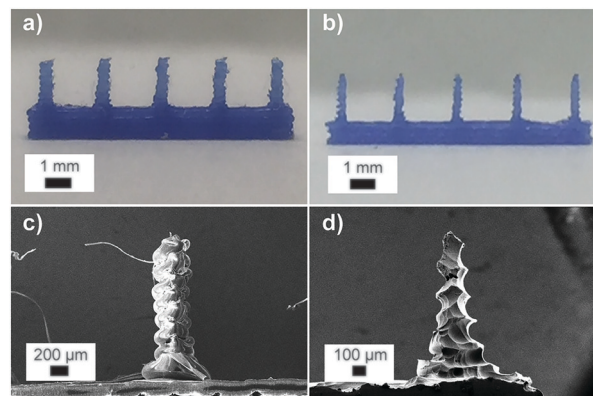









Fig. 2 Optical images of microneedles a) as fabricated and b) after etching. SEM images of microneedles c) as fabricated and d) after etching.

in size over time (Fig. S2 and S3†). After 9 hours with 5 M KOH, the MNs remained approximately the same length; however, the thickness and width decreased to a range between 200–300 μm with a tip size between 1–55 μm (Fig. 2b–d), which are within the optimal range for painless MNs. Differential scanning calorimetry (DSC) measurements found no differences between etched and unetched MNs (Fig. S4†). Intriguingly, we found the needles were barbed shaped as a result of the layer-by-layer deposition process, which would help prevent the needles from falling out of the skin after insertion.

Needle density is a parameter of MN array design. While closely packing microneedles increases the drug loading capacity, higher density designs tend to cause more pain.⁶⁷ Additionally, higher density needle arrays are difficult to fabricate using FDM. To test these limits, a series of array designs, which varied the needle lengths and densities, were printed on a 1 cm^2 base. The lengths chosen for types 1–3 were the upper and lower limit of currently produced MNs, which are 0.6 and 1.4 mm. We found we could make 6 \times 6 MN arrays reproducibly on a 1 cm^2 base (Fig. S5†). Lithographically producing all the templates required to make comparable MN arrays would have taken days; whereas, we were able to produce custom designed MNs in only a few hours.

Axial and transverse fracture tests and a bend baseplate test were conducted following modified procedures of Woolfson *et al.*⁶⁹ The axial fracture test applies a force perpendicular to the MN until a dip occurs, which is called the fracture failure point (Fig. S6a and b and S7a and b†). The rate of the moving arm was 300 $\mu\text{m s}^{-1}$ to obtain a force of 0.23 N at the point of fracture, which is above the 0.058 N that is required to pierce through the top layer of skin, a 10–20 μm thickness known as the *stratum corneum*.⁷⁰ The transverse fracture test applies a force parallel to the MN until the fracture failure point (Fig. S6c and d†). This shows the amount of force the needles can withstand before breaking sideways (Fig. S8a and b†). At a rate of 300 $\mu\text{m s}^{-1}$, we

Table 1 Microneedle designs tested with the 3D printer

Array	Shape	Printer	Etch	Parafilm	Skin
Type 1		✗	✗	✗	✗
Type 2		✗	✗	✗	✗
Type 3		✗	✗	✗	✗
Type 4		✗	✗	✗	✗
Type 5		✓	✓	✓	✗
Type 6		✓	✓	✓	✗
Type 7		✓	✓	✓	✓

obtained 0.64 N for our etched MNs. These results, in combination with the DSC, shows that etching the needles does not affect the mechanical and material properties of PLA—similar to currently fabricated MNs.^{35,70} All needles fractured in each test were verified optically and these results are tabulated in Table S1†. Because FDM prints layers of plastic, we can easily adjust the thickness—and presumably the flexibility—of the base by changing the number of printed layers (Fig. S9†). To that end, a base plate test was conducted for bases produced with two, three, and four layers of PLA (Table S2†). We obtained 15.6° for the four layers before the base broke in half (Fig. S10†). This is far more flexible than reported⁶⁹ values of bases made from poly(lactic-co-glycolic) acid using conventional molds, which break at 1.28°. The flexibility allows the MN array to easily deform when applied to any surface on the body.

The performance of the etched MNs in transdermal drug delivery was evaluated *via* penetration and staining test. We initially tested penetration on a 1.8 mm thick sheet of parafilm, which has been shown to mimic the mechanical properties of skin.⁷¹ Etched MN arrays 1.4 mm in length were inserted perpendicular into the parafilm and were broken off by applying transverse force after insertion with a success rate of 92% (Fig. 3a). In other words, 92% of the needles on the array successfully pierced the parafilm and remained imbedded in the film following transverse pressure to break them off. This was further tested with MNs with lengths of 0.6, 1.0, and 1.2 mm. Similar results were obtained for 1.2 mm needles, however, 0.6 mm and 1.0 mm failed to break off. While useful for mechanical testing, parafilm does not mimic the physiological environment of skin and not adequate to measure drug diffusion.

Porcine skin was used as a physiological mimic of human skin and was cut into 3 × 3 cm slabs. The insertion of MNs

1.4 mm in length into porcine skin, followed by application of transverse force resulted in 84% of the needles breaking away from the array and remaining embedded in the tissue. This was also tested with the shorter length MNs, which demonstrated penetration but again did not break-off with transverse force. These results are in line with published dissolvable MNs made *via* photolithography (Fig. 3b and c).^{72,73} Cross-sectional measurements at the location of insertion of the 1.4 mm MNs confirmed insertion and showed depths up to 250 μm (Fig. 3d).

A key quality of these needles is that they can be used as solid, coated, or dissolvable MNs. Drugs can be loaded by coating the needles or encapsulation within the polymer matrix. To assess our etched MNs for drug delivery by coating we used methylene blue, followed by insertion into porcine skin. The MNs remained in the porcine skin to allow the absorption of methylene blue to diffuse into the tissue and were removed after 30 s. The tissue was then optically imaged (Fig. 3e and f) and the expected transfer of methylene blue was seen in the perforated tissue.

While coated MNs are easy to prepare, drug loading is limited and release rates are difficult to control. A more sophisticated architecture to control drug release and improve loading is to absorb drugs into the polymeric matrix of a dissolvable MN array. Previous results⁶⁵ have shown that PLA sutures degrade in physiological environments. It stands to reason that small molecules embedded in polymer matrix should be released as the PLA MNs dissolve. To load our drug-like molecule—we used fluorescein in these tests—we identified solvents capable of swelling, but not dissolving PLA. To load our needles, arrays were soaked in an acetone solution containing 2 mg mL⁻¹ of fluorescein for 1 h. Acetone was then removed from the MN arrays by evaporation for 30 min under dynamic vacuum (Fig. S11†). We tested drug

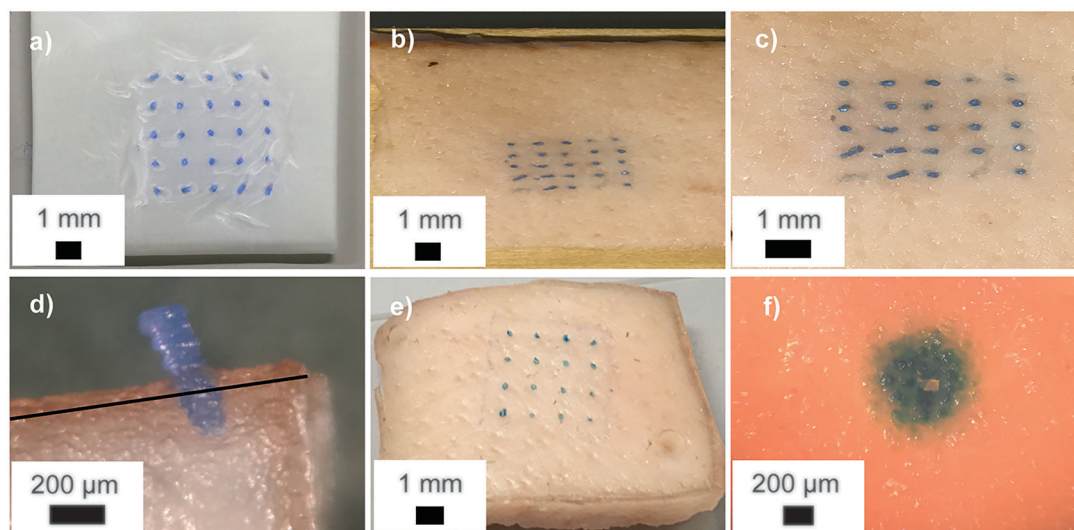


Fig. 3 Fracture test of microneedles a) in parafilm, b) in porcine skin, c) zoomed in image of porcine skin, and d) cross-section image indicating needle penetration depth in porcine skin. The solid line represents the end of the *stratum corneum*. Penetration test of microneedles e) to demonstrate the diffusion of methylene blue in the porcine skin and f) close up image of a single puncture showing delivery in the surrounding tissue.

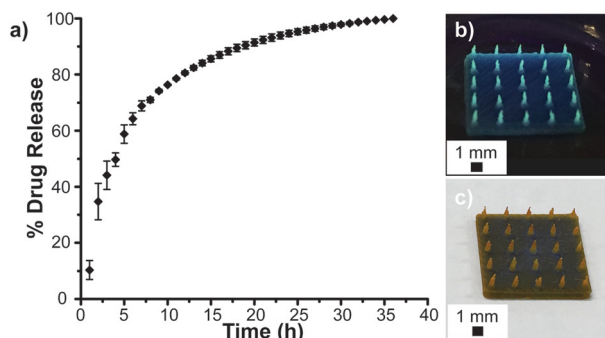


Fig. 4 The release of microneedles containing fluorescein in a solution of buffer at pH 4 a) monitored over 36 h b) fluorescent microneedles under UV light (365 nm) c) loaded microneedles after solvent removal.

release under pH conditions representative of those found in the skin. Our general procedure involved submerging 100 individual MNs (equivalent to four MN arrays) in sodium acetate/acetic acid buffer solution (pH 4.0) to simulate needles broken off into the skin. The release of fluorescein was monitored by UV-vis spectroscopy (Fig. 4a) for 36 hours and the drug concentrations per MN array were calculated using the Beer-Lambert law (Fig. S12[†]). We have demonstrated that 3.23 μg of the model drug can be delivered from 25 needles (a single MN array, Fig. 4b and c and S13[†]), with 50% drug release occurring after approximately 4 h.

Fluorescent MN arrays were inserted into porcine skin samples to visualize release and diffusion over time (Fig. 5). Shortly after insertion, fluorescein was localized at the site of penetration (Fig. 5a) and over time the fluorescein began to diffuse as seen in Fig. 5b–d. It should be noted that after 12 h further diffusion of fluorescein was minimal as approximately 80% had been released. Cross-sections of porcine samples at the site of insertion were imaged to determine the extent of fluorescein diffusion over time (Fig. 5e–h). As expected, the fluorescein diffused evenly throughout the por-

cine skin as time progressed. This diffusion behaviour verifies the MNs ability to penetrate past the *stratum corneum* and facilitate passive drug delivery.

Conclusions

In summary, we have developed a new chemical etching method that improves the feature size resolution of FDM printed materials allowing for the fabrication of biocompatible MNs capable of penetrating the outer layers of skin and delivering a model therapeutic agent. We have shown that printing parameters can easily be tuned to develop MNs of varying shapes, lengths, and array densities without the need of a master template. While PLA, a polyester derived from renewable monomers, is a common filament choice for FDM printing, other polyesters have been investigated for uses in tissue engineering,⁷⁴ blends to enhance properties,^{75–77} and other medical applications.⁷⁸ Furthermore, FDM is compatible with other biorenewable thermoplastic materials that are FDA approved such as polyglycolic acid, polycaprolactone, and poly(lactic-co-glycolic) acid. Using our etching method, all of these biocompatible polyesters—which currently cannot be used with higher resolution printing techniques such as SLA—could now be applied in MN fabrication. Future work involves improving the FDM 3D printer's nozzle design to enhance the resolution without raising the cost significantly or developing a technique that will allow for more versatile MNs. By enhancing the resolution, more defined shapes can be made, which would lower the amount of time needed for etching. With the advancement of 3D printing in industry, particularly recent commercial launches of 3D printed products, this method provides a scalable fabrication of MNs. This novel fabrication method has demonstrated the potential of rapid prototyping MNs at low costs, bridging the gap between additive manufacturing and passive drug delivery.

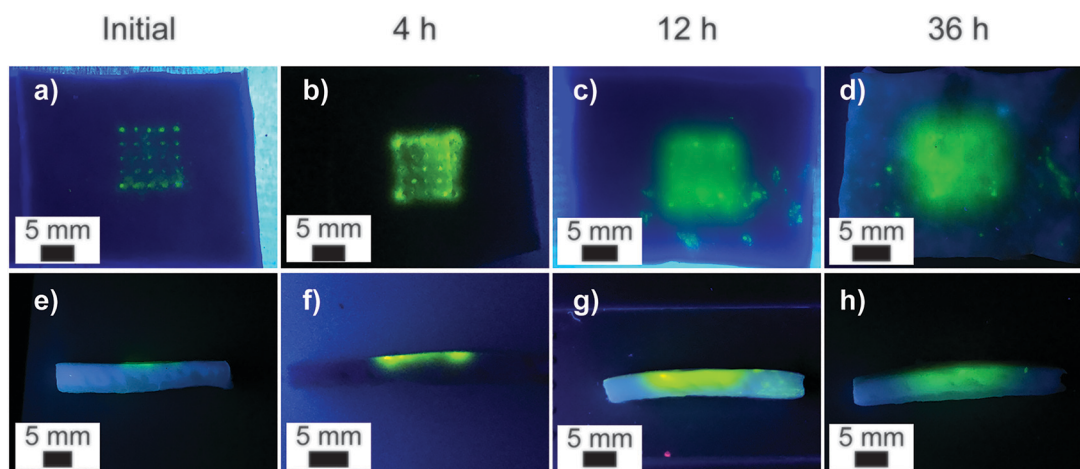


Fig. 5 Images of porcine samples inserted with loaded microneedles a) after initial insertion, b) 4 h, c) 12 h, and d) 36 h. Images of cross-sections of porcine samples e) after initial insertion, f) 4 h, g) 12 h, and h) 36 h. All images were illuminated by a 15 W UV (365 nm) light.

Experimental

Materials

Fluorescein, acetone, and potassium hydroxide were purchased from Sigma Aldrich or Fisher Scientifics and used as received without further purification. Porcine skin was purchased from Sierra for Medical Science. Polylactic acid filament was purchased from SUNLU.

Fabrication of 3D printed microneedles

Types 1–7 MNs were designed using the Blender software package and fabricated using a LulzBot TAZ 5 3D printer (Aleph Object, Inc., Loveland, CO) with 3.0 mm PLA filament (Zhunhai Sunlu Industrial Co., LTD). The printer was operated with the Cura software package for LulzBot. The printing parameters used to fabricate MNs are as such: print speed: 50 mm s⁻¹, layer height: 0.2 mm, shell thickness: 0.30 mm, retraction speed: 10 mm s⁻¹, travel speed: 175 mm s⁻¹, bottom layer speed: 15 mm s⁻¹, infill speed: 30 mm s⁻¹, top/bottom speed: 20 mm s⁻¹, outer shell speed: 20 mm s⁻¹, and inner shell speed: 20 mm s⁻¹. The temperature of the hot end was set at 195 °C, and the temperature of the print bed was set to 60 °C. A print head with a 0.35 mm nozzle diameter was used.

Microneedle array etching and loading

As fabricated MNs made from PLA were placed in a 5 M KOH bath for 4 h, such that only the needle tips were submerged. After 4 h, the MN arrays were completely immersed for an additional 5 h followed by several washes with water to remove the KOH solution. To load fluorescein, etched MN arrays were immersed in an acetone solution containing fluorescein (2 mg mL⁻¹) for 1 h. Acetone was then removed from the MN arrays by evaporation for 30 min under dynamic vacuum.

Mechanical testing of MN arrays

All mechanical properties were performed on a Instron 5848 Micro Tester (Illinois Tool Works, Inc, Norwood, MA). The moving arm in all test moved at 300 μm s⁻¹. For axial fracture test, MNs were placed directly on the loading cell and a cylindrical probe was used to apply an axial force. For the transverse fracture test, an aluminium block was used (Fig. S9 and S10†). The backing layer of the MN array was attached with ethyl cyanoacrylate super glue gel (Harbor Freight Tools, Caramillo, CA). A metal probe with a 1 cm blunt end was used to apply a transverse force on the needle. For bend test, two aluminium blocks were used to hold the MN array above the loading cell (Fig. S10†). The probe was then used to apply force on the center of the backing layer.

Porcine skin cargo delivery tests

Porcine skin (Sierra for Medical Science) was cut into 3 × 3 cm slabs and nailed to a wooden block. For needle fracture testing, etched MNs were inserted perpendicular to the porcine skin and transverse force was applied until needle frac-

ture occurred. To test the delivery of cargo that was coated onto the MNs, methylene blue was applied on the needles. Tweezers were used to hold the backing layer to submerge only the needle tips into the dye. The coated needles were then inserted into porcine skin for 30 s, and delivery into porcine skin was verified with an optical microscope (AmScope SE306R-PZ). To test the diffusion rate and efficacy of fluorescein from the MNs into porcine skin tissue, the MN arrays were inserted into to the porcine skin and removed after initial insertion, 4, 12, and 36 h under ambient conditions without shearing the needles. Images were taken under ambient and ultraviolet light (365 nm).

Characterization

All MNs were imaged using scanning electron microscopy (SEM, LEO, 1530, Zeiss) with an accelerating voltage of 2.5 kV. To enhance the conductivity, the samples were treated with gold sputtering method prior to microscope characterization.

UV-vis drug release tests were performed using a Cary 5000 UV-vis-NIR spectrophotometer (Agilent, Santa Clara, CA). MNs loaded with fluorescein were removed from the base of four MN arrays (100 needles) and placed into a quartz cuvette with a 1 cm path length. The cuvette was filled with sodium acetate/acetic acid buffer (3.3 mL, pH 4) and measured in 1 h intervals for 36 h. The samples were agitated before each measurement for the first 6 h.

Author contribution

All authors have given approval to the final version of the manuscript. M. A. L., R. A. S., and J. J. G. designed and conducted the experiments; M. A. L. and J. C. R. optimized parameters for the 3D printed microneedles; M. A. L. developed etching protocol, took SEM images, performed the mechanical properties, and time studies of fluorescein diffusion into porcine skin; M. A. L. and D. R. B. did porcine insertions; D. R. B. loaded microneedles with fluorescein and conducted the kinetics studies.

Conflicts of interest

There are no conflicts to declare.

Acknowledgements

R. A. S. acknowledges support from the Department of Energy's Kansas City National Security Campus, which is operated and managed by Honeywell FM&T, LLC, for the National Nuclear Security Administration. J. J. G. acknowledges the National Science Foundation (DMR-1654405) for funding.

References

- 1 B. Deacon and J. Abramowitz, *J. Anxiety Disord.*, 2006, **20**, 946–960.

- 2 R. Hanas, *Pediatr. Diabetes*, 2004, 5, 102–111.
- 3 S. Henry, D. V. McAllister, M. G. Allen and M. R. Prausnitz, *J. Pharm. Sci.*, 1998, 87, 922–925.
- 4 R. F. Donnelly, T. R. R. Singh and A. D. Woolfson, *Drug Delivery*, 2010, 17, 187–207.
- 5 P. Ghosh, N. K. Brogden and A. L. Stinchcomb, *J. Pharm. Sci.*, 2014, 103, 652–660.
- 6 H.-W. Yang, L. Ye, X. D. Guo, C. Yang, R. W. Compans and M. R. Prausnitz, *Adv. Healthcare Mater.*, 2017, 6, 1600750.
- 7 J. M. Arya, K. Dewitt, M. Scott-Garrard, Y.-W. Chiang and M. R. Prausnitz, *J. Controlled Release*, 2016, 239, 19–26.
- 8 P. C. DeMuth, A. V. Li, P. Abbink, J. Liu, H. Li, K. A. Stanley, K. M. Smith, C. L. Lavine, M. S. Seaman, J. A. Kramer, A. D. Miller, W. Abraham, H. Suh, J. Elkhader, P. T. Hammond, D. H. Barouch and D. J. Irvine, *Nat. Biotechnol.*, 2013, 31, 1082–1085.
- 9 Z. Zhu, X. Ye, Z. Ku, Q. Liu, C. Shen, H. Luo, H. Luan, C. Zhang, S. Tian, C. Lim, Z. Huang and H. Wang, *J. Controlled Release*, 2016, 243, 291–302.
- 10 A. K. Shakya, C. H. Lee and H. S. Gill, *J. Controlled Release*, 2017, 265, 75–82.
- 11 R. F. Donnelly, T. R. R. Singh, M. M. Tunney, D. I. J. Morrow, P. A. McCarron, C. O'Mahony and A. D. Woolfson, *Pharm. Res.*, 2009, 26, 2513–2522.
- 12 R. F. Donnelly, K. Moffatt, A. Z. Alkilani, E. M. Vicente-Pérez, J. Barry, M. T. C. McCrudden and A. D. Woolfson, *Pharm. Res.*, 2014, 31, 1989–1999.
- 13 J. C. Birchall, R. Clemo, A. Anstey and D. N. John, *Pharm. Res.*, 2011, 28, 95–106.
- 14 D. Kristensen, D. Chen and R. Cummings, *Vaccine*, 2011, 29, 7122–7124.
- 15 Y. Hiraishi, T. Nakagawa, Y.-S. Quan, F. Kamiyama, S. Hirobe, N. Okada and S. Nakagawa, *Int. J. Pharm.*, 2013, 441, 570–579.
- 16 E. S. Esser, J. A. Pulit-Penalzoza, H. Kalluri, D. McAllister, E. V. Vassilieva, E. Q. Littauer, N. Lelutiu, M. R. Prausnitz, R. W. Compans and I. Skountzou, *Sci. Rep.*, 2017, 7, 5705.
- 17 S. Li, M. Dharmarwardana, R. P. Welch, Y. Ren, C. M. Thompson, R. A. Smaldone and J. J. Gassensmith, *Angew. Chem.*, 2016, 128, 10849–10854.
- 18 Z. Chen, N. Li, L. Chen, J. Lee and J. J. Gassensmith, *Small*, 2016, 12, 4563–4571.
- 19 Y. Zhang, J. Yu, J. Wang, N. J. Hanne, Z. Cui, C. Qian, C. Wang, H. Xin, J. H. Cole, C. M. Gallippi, Y. Zhu and Z. Gu, *Adv. Mater.*, 2017, 29, 1604043.
- 20 L. Y. Chu and M. R. Prausnitz, *J. Controlled Release*, 2011, 149, 242–249.
- 21 K. Lee, C. Y. Lee and H. Jung, *Biomaterials*, 2011, 32, 3134–3140.
- 22 J. Yu, Y. Zhang, Y. Ye, R. DiSanto, W. Sun, D. Ranson, F. S. Ligler, J. B. Buse and Z. Gu, *Proc. Natl. Acad. Sci. U. S. A.*, 2015, 112, 8260–8265.
- 23 R. F. Donnelly, T. R. R. Singh, M. J. Garland, K. Migalska, R. Majithiya, C. M. McCrudden, P. L. Kole, T. M. T. Mahmood, H. O. McCarthy and A. D. Woolfson, *Adv. Funct. Mater.*, 2012, 22, 4879–4890.
- 24 A. Nayak and D. B. Das, *Biotechnol. Lett.*, 2013, 35, 1351–1363.
- 25 J. Chen, Y. Qiu, S. Zhang, G. Yang and Y. Gao, *Drug Dev. Ind. Pharm.*, 2015, 41, 415–422.
- 26 G. Du, R. M. Hathout, M. Nasr, M. R. Nejadnik, J. Tu, R. I. Koning, A. J. Koster, B. Slütter, A. Kros, W. Jiskoot, J. A. Bouwstra and J. Mönkäre, *J. Controlled Release*, 2017, 266, 109–118.
- 27 J. McCaffrey, R. F. Donnelly and H. O. McCarthy, *Drug Delivery Transl. Res.*, 2015, 5, 424–437.
- 28 N. S. Rejinold, J.-H. Shin, H. Y. Seok and Y.-C. Kim, *Expert Opin. Drug Delivery*, 2016, 13, 109–131.
- 29 H. Kalluri, C. S. Kolli and A. K. Banga, *AAPS J.*, 2011, 13, 473–481.
- 30 E. Larrañeta, R. E. M. Lutton, A. D. Woolfson and R. F. Donnelly, *Mater. Sci. Eng., R*, 2016, 104, 1–32.
- 31 W. Chen, H. Li, D. Shi, Z. Liu and W. Yuan, *Front. Pharmacol.*, 2016, 7, 137.
- 32 S. Yang, Y. Feng, L. Zhang, N. Chen, W. Yuan and T. Jin, *Int. J. Nanomed.*, 2012, 7, 1415–1422.
- 33 Y. Ye, J. Yu, D. Wen, A. R. Kahkoska and Z. Gu, *Adv. Drug Delivery Rev.*, 2018, DOI: 10.1016/j.addr.2018.01.015.
- 34 S. Yang, F. Wu, J. Liu, G. Fan, W. Welsh, H. Zhu and T. Jin, *Adv. Funct. Mater.*, 2015, 25, 4633–4641.
- 35 J.-H. Park, M. G. Allen and M. R. Prausnitz, *J. Controlled Release*, 2005, 104, 51–66.
- 36 L. Y. Chu, S.-O. Choi and M. R. Prausnitz, *J. Pharm. Sci.*, 2010, 99, 4228–4238.
- 37 J. A. Rogers, Z. Bao, K. Baldwin, A. Dodabalapur, B. Crone, V. R. Raju, V. Kuck, H. Katz, K. Amundson, J. Ewing and P. Drzaic, *Proc. Natl. Acad. Sci. U. S. A.*, 2001, 98, 4835–4840.
- 38 S. D. Gittard, A. Ovsianikov, N. A. Monteiro-Riviere, J. Lusk, P. Morel, P. Minghetti, C. Lenardi, B. N. Chichkov and R. J. Narayan, *J. Diabetes Sci. Technol.*, 2009, 3, 304–311.
- 39 E. Parker, M. Rao, K. Turner, C. Meinhart and N. MacDonald, *J. Microelectromech. Syst.*, 2007, 16, 289–295.
- 40 N. Guo and M. C. Leu, *Front. Mech. Eng.*, 2013, 8, 215–243.
- 41 K. Henke and S. Treml, *Eur. J. Wood Wood Prod.*, 2013, 71, 139–141.
- 42 M. Richardson and B. Haylock, *Comput. Aided Des. Appl.*, 2012, 2, 33–48.
- 43 N. A. Ahmed and J. R. Page, *Appl. Mech. Mater.*, 2013, 397, 970–980.
- 44 D. M. Kirchmayer and R. Gorkin III, *J. Mater. Chem. B*, 2015, 3, 4105–4117.
- 45 L. R. Hart, S. Li, C. Sturgess, R. Wildman, J. R. Jones and W. Hayes, *ACS Appl. Mater. Interfaces*, 2016, 8, 3115–3122.
- 46 C. S. Lee, S. G. Kim, H. J. Kim and S. H. Ahn, *J. Mater. Process. Technol.*, 2007, 187, 627–630.
- 47 M. D. Symes, P. J. Kitson, J. Yan, C. J. Richmond, G. J. T. Cooper, R. W. Bowman, T. Vilbrandt and L. Cronin, *Nat. Chem.*, 2012, 4, 349–354.
- 48 P. J. Kitson, G. Marie, J.-P. Francoia, S. S. Zalesskiy, R. C. Sigerson, J. S. Mathieson and L. Cronin, *Science*, 2018, 359, 314–319.
- 49 G. Comina, A. Suska and D. Filippini, *Lab Chip*, 2014, 14, 2978–2982.

- 50 J. R. Davidson, G. A. Appuhamillage, C. M. Thompson, W. Voit and R. A. Smaldone, *ACS Appl. Mater. Interfaces*, 2016, 8, 16961–16966.
- 51 G. A. Appuhamillage, J. C. Reagan, S. Khorsandi, J. R. Davidson, W. Voit and R. A. Smaldone, *Polym. Chem.*, 2017, 8, 2087–2092.
- 52 K. Yang, J. C. Grant, P. Lamey, A. Joshi-Imre, B. R. Lund, R. A. Smaldone and W. Voit, *Adv. Funct. Mater.*, 2017, 27, 1700318.
- 53 Y. He, G.-H. Xue and J.-Z. Fu, *Sci. Rep.*, 2014, 4, 6973.
- 54 C. Schubert, M. C. van Langeveld and L. A. Donoso, *Br. J. Ophthalmol.*, 2014, 98, 159.
- 55 D. Zhang, B. Chi, B. Li, Z. Gao, Y. Du, J. Guo and J. Wei, *Synth. Met.*, 2016, 217, 79–86.
- 56 D. W. Hutmacher, T. Schantz, I. Zein, K. W. Ng, S. H. Teoh and K. C. Tan, *J. Biomed. Mater. Res., Part A*, 2001, 55, 203–216.
- 57 I. Zein, D. W. Hutmacher, K. C. Tan and S. H. Teoh, *Biomaterials*, 2002, 23, 1169–1185.
- 58 A. Döpp, E. Guillaume, C. Thauray, J. Gautier, K. Ta Phuoc and V. Malka, *Rev. Sci. Instrum.*, 2016, 87, 073505.
- 59 B. Caulfield, P. E. McHugh and S. Lohfeld, *J. Mater. Process. Technol.*, 2007, 182, 477–488.
- 60 S. A. Skoog, P. L. Goering and R. J. Narayan, *J. Mater. Sci.: Mater. Med.*, 2014, 25, 845–856.
- 61 Z. F. Rad, R. E. Nordon, C. J. Anthony, L. Bilston, P. D. Prewett, J.-Y. Arns, C. H. Arns, L. Zhang and G. J. Davies, *Microsyst. Nanoeng.*, 2017, 3, 17034.
- 62 T. Matsuda and M. Mizutani, *J. Biomed. Mater. Res.*, 2002, 62, 395–403.
- 63 A. R. Johnson, C. L. Caudill, J. R. Tumbleston, C. J. Bloomquist, K. A. Moga, A. Ermoshkin, D. Shirvanyants, S. J. Mecham, J. C. Luft and J. M. DeSimone, *PLoS One*, 2016, 11, e0162518.
- 64 S. H. Lim, J. Y. Ng and L. Kang, *Biofabrication*, 2017, 9, 015010.
- 65 K. A. Athanasiou, G. G. Niederauer and C. M. Agrawal, *Biomaterials*, 1996, 17, 93–102.
- 66 S. Kaushik, A. H. Hord, D. D. Denson, D. V. McAllister, S. Smitra, M. G. Allen and M. R. Prausnitz, *Anesth. Analg.*, 2001, 92, 502–504.
- 67 H. S. Gill, D. D. Denson, B. A. Burris and M. R. Prausnitz, *Clin. J. Pain*, 2008, 24, 585–594.
- 68 G. Yosipovitch, G. L. Xiong, E. Haus, L. Sackett-Lundeen, I. Ashkenazi and H. I. Maibach, *J. Invest. Dermatol.*, 1998, 110, 20–23.
- 69 R. F. Donnelly, R. Majithiya, T. R. R. Singh, D. I. J. Morrow, M. J. Garland, Y. K. Demir, K. Migalska, E. Ryan, D. Gillen, C. J. Scott and A. D. Woolfson, *Pharm. Res.*, 2011, 28, 41–57.
- 70 K. J. Cha, T. Kim, S. J. Park and D. S. Kim, *J. Micromech. Microeng.*, 2014, 24, 115015.
- 71 E. Larrañeta, J. Moore, E. M. Vicente-Pérez, P. González-Vázquez, R. Lutton, A. D. Woolfson and R. F. Donnelly, *Int. J. Pharm.*, 2014, 472, 65–73.
- 72 J. S. Kochhar, P. Anbalagan, S. B. Shelar, J. K. Neo, C. Iliescu and L. Kang, *Pharm. Res.*, 2014, 31, 1724–1734.
- 73 S. F. Lahiji, M. Dangol and H. Jung, *Sci. Rep.*, 2015, 5, 7914.
- 74 A. Basu, K. R. Kunduru, S. Doppalapudi, A. J. Domb and W. Khan, *Adv. Drug Delivery Rev.*, 2016, 107, 192–205.
- 75 V. H. Sangeetha, H. Deka, T. O. Varghese and S. K. Nayak, *Polym. Compos.*, 2018, 39, 81–101.
- 76 Y. Xu, J. Loi, P. Delgado, V. Topolkaev, R. J. McEneaney, C. W. Macosko and M. A. Hillmyer, *Ind. Eng. Chem. Res.*, 2015, 54, 6108–6114.
- 77 N. J. Van Zee and G. W. Coates, *Angew. Chem., Int. Ed.*, 2015, 54, 2665–2668.
- 78 M. A. Ghalia and Y. Dahman, *J. Polym. Res.*, 2017, 24, 74.